





## Article

# Sugarcane Bagasse Ash as a Catalyst Support for Facile and Highly Scalable Preparation of Magnetic Fenton Catalysts for Ultra-Highly Efficient Removal of Tetracycline

Natthanan Rattanachueskul <sup>1</sup>, Oraya Dokkathin <sup>1</sup>, Decha Dechtrirat <sup>2,3,4</sup>, Joongjai Panpranot <sup>5</sup>, Waralee Watcharin <sup>6</sup>, Sulawan Kaowphong <sup>7</sup> and Laemthong Chuenchom <sup>1,\*</sup>

- <sup>1</sup> Division of Physical Science (Chemistry Program) and Center of Excellence for Innovation in Chemistry, Faculty of Science, Prince of Songkla University, Hat-Yai District, Songkhla 90110, Thailand; natthanan.rc@gmail.com (N.R.); orayamod.d@gmail.com (O.D.)
- <sup>2</sup> Department of Materials Science, Faculty of Science, Kasetsart University, Bangkok 10900, Thailand; fscidcd@ku.ac.th
- <sup>3</sup> Specialized Center of Rubber and Polymer Materials for Agriculture and Industry (RPM), Faculty of Science, Kasetsart University, Bangkok 10900, Thailand
- <sup>4</sup> Laboratory of Organic Synthesis, Chulabhorn Research Institute, Bangkok 10210, Thailand
- <sup>5</sup> Department of Chemical Engineering, Faculty of Engineering, Chulalongkorn University, Bangkok 10330, Thailand; joongjai.p@chula.ac.th
- <sup>6</sup> Faculty of Biotechnology (Agro-Industry), Assumption University, Hua Mak Campus, Bangkok 10240, Thailand; waraleewtc0@gmail.com
- <sup>7</sup> Department of Chemistry and Center of Excellence in Materials Science and Technology, Faculty of Science, Chiang Mai University, Chiang Mai 50200, Thailand; sulawank@gmail.com
- \* Correspondence: laemthong.c@psu.ac.th; Tel.: +66-74-288416; Fax: +66-74-558841



**Citation:** Rattanachueskul, N.; Dokkathin, O.; Dechtrirat, D.; Panpranot, J.; Watcharin, W.; Kaowphong, S.; Chuenchom, L. Sugarcane Bagasse Ash as a Catalyst Support for Facile and Highly Scalable Preparation of Magnetic Fenton Catalysts for Ultra-Highly Efficient Removal of Tetracycline. *Catalysts* **2022**, *12*, 446. <https://doi.org/10.3390/catal12040446>

Academic Editors: Sagadevan Suresh and Is Fatimah

Received: 14 March 2022

Accepted: 14 April 2022

Published: 18 April 2022

**Publisher's Note:** MDPI stays neutral with regard to jurisdictional claims in published maps and institutional affiliations.



**Copyright:** © 2022 by the authors. Licensee MDPI, Basel, Switzerland. This article is an open access article distributed under the terms and conditions of the Creative Commons Attribution (CC BY) license (<https://creativecommons.org/licenses/by/4.0/>).

**Abstract:** Sugarcane bagasse ash, which is waste from the combustion process of bagasse for electricity generation, was utilized as received as a catalyst support to prepare the magnetic sugarcane bagasse ash (MBGA) with different iron-to-ash ratios using a simple co-precipitation method, and the effects of NaOH and iron loadings on the physicochemical properties of the catalyst were investigated using various intensive characterization techniques. In addition, the catalyst was used with a low amount of H<sub>2</sub>O<sub>2</sub> for the catalytic degradation of a high concentration of tetracycline (800 mg/L) via a Fenton system. The catalyst exhibited excellent degradation activity of 90.43% removal with good magnetic properties and high stabilities and retained good efficiency after four cycles with NaOH as the eluent. Moreover, the hydroxyl radical on the surface of catalyst played a major role in the degradation of TC, and carbon-silica surface of bagasse ash significantly improved the efficiencies. The results indicated that the MBGA catalyst shows the potential to be highly scalable for a practical application, with high performance in the heterogeneous Fenton system.

**Keywords:** heterogeneous Fenton; tetracycline removal; magnetite; sugarcane bagasse ash

## 1. Introduction

Tetracycline (TC), the pharmaceutical antibiotic, has been widely used in many fields such as human and livestock feeding. The TC contaminative wastewater from hospitals and pharmaceutical industries is considered a threat to the aquatic system and human health due to its exposure to microorganisms causing drug resistance [1–3]. Therefore, it is imperative to efficiently remove TC from wastewater before discharge.

Various methods have been used to remove TC from aqueous systems. Adsorption is among the most popular techniques [4–6]; however, although it shows high TC removal efficiency, TC residue is still trapped inside the adsorbents, and so it only changes the location of TC. Coagulation is another method to remove TC from wastewater [7,8]. Nevertheless, it requires large amounts of expensive chemicals, resulting in overall costly operation.

Furthermore, after adsorption and coagulation processes, both the TC-loaded adsorbents and TC-contaminated coagulants are defined as hazardous wastes, which leads to difficulty in post-processing.

For the above reasons, alternative methods to efficiently remove TC from the water system are still highly required. Advance oxidation processes (AOPs) are a kind of chemical technology which degrades organic pollutants using highly reactive species such as hydroxyl radicals ( $\cdot\text{OH}$ ). The OH radicals generated from AOPs can convert toxic organic compounds in a non-selective way into the non-toxic inorganic products. Therefore, the AOPs have become more attractive [1,9,10]. One of the most attractive AOPs which can be operated at ambient temperatures and pressures is the Fenton process because of its high degradation efficiency, simple and low-cost operation, and mild and green reaction conditions [1,9–11].

The classical Fenton reagent consists of iron salts and hydrogen peroxide ( $\text{H}_2\text{O}_2$ ) as an oxidant in a homogeneous solution. However, the iron sludge produced after the treatment is the main drawback of this homogenous catalyst, which is difficult to separate and can be secondary contaminant to the treated water [9,10,12].

To solve this problem, heterogeneous Fenton processes using magnetic solid iron-based catalysts have received broad attention for the elimination of various types of organic pollutants [13–16].

The inverse spinel  $\text{Fe}_3\text{O}_4$  (magnetite) is one of the most studied magnetic particles, which can be used for a wide range of applications such as adsorption [17–21] and catalysis [15,22–25]. Many previous reports revealed its highly efficient catalytic performance in a heterogeneous Fenton system, where  $\text{Fe}^{2+}$  in magnetite structure can play a main role in initiating the Fenton reaction in the presence of  $\text{H}_2\text{O}_2$  according to the classical Haber–Weiss mechanism [11,26–28]. With the presence of both  $\text{Fe}^{2+}$  and  $\text{Fe}^{3+}$ , this allows the Fe ions to be oxidized and reduced in a reversible loop and be kept reactive in the Fenton system. Additionally, the magnetite particles possess strong magnetic properties; therefore, they are considered suitable as a heterogeneous Fenton catalyst with rapid and effective separation from aqueous solution using an external magnet.

However, the surface area is considered an important factor in a heterogeneous reaction, while the surface area of magnetite particles is generally low. To enhance the catalytic activity of magnetite particles, the magnetic solid iron-based catalysts on supports such as silica [1,9,29,30], and carbonaceous materials [1,13,31–33] have widely been investigated due to their high stability, low toxicity, wide availability, and low-cost materials. Nevertheless, the preparation techniques of those catalysts are complex and rely on multi-step processes, including use of harmful chemicals and high temperatures [34–38]. Moreover, the concentration of TC studied by many works is still comparatively low (<50 ppm), while the catalyst dosages are comparatively high (0.5–1.0 g/L). This indicates that the actual amount of TC in the solution for those studies was considered very low (0.2–10 mg).

The fact that no one reports on the removal efficiency for catalytic degradation in terms of real absolute TC amount in mg leads to difficulty when comparing the performance of catalyst with other works. Herein, the amount of TC removal per catalyst dosage was calculated in this work to be compared clearly among literature reviews.

Sugarcane bagasse ash (BGA) is the remaining waste from the combustion process of sugarcane bagasse for generation of electricity, which is considered as the simplest and most cost-effective utilization of bagasse [39,40]. Because Thailand is one of the largest sugar producers in the world, there is still a huge amount of sugarcane bagasse ash left from the combustion process (around 365,000 tons/year) [41–43]. In fact, a common utilization of this solid waste is mainly landfill disposal, which is unsustainable for the circular economy concept [44]. Moreover, without the right care, the obtained fly ash—which is considered particulate matter—can cause air pollution, leading to respiratory diseases [45,46].

Many researchers have used it as a substitute component for building material [47–49] or as fertilizer to improve agricultural productivity [50,51], or directly used it as an adsorbent for wastewater treatment [52–54].

However, the obtained sugarcane bagasse ash with a high surface area and chemical stabilities is a promising material for catalyst support, and to the best of our knowledge, only a few studies have been found on using ash as catalyst supports [24,30,55]. Moreover,  $\text{Fe}_3\text{O}_4$ @ash from sugarcane bagasse has not been previously studied as a Fenton catalyst for the removal of organic pollutants.

Generally, catalyst support can be obtained from multiple-step synthesis, not from as-received precursors. This escalates more steps into the whole synthesis pathway. These supports should be environmentally friendly, cost effective, sustainable, and have high stability. BGA is typically obtained as waste through incomplete combustion of sugarcane bagasse during the process of generation of electricity in biomass power plants. Unlike other types of ashes, the main characteristic of BGA is the presence of high carbon and silica content and suitable textural morphology. The presence of those elements, as well as the high surface area of non-toxic BGA, can provide properties similar to those of good catalyst supports without any pretreatment process. With the simple one-step co-precipitation method, magnetic sugarcane bagasse ash can be prepared, which is easy and scalable. Moreover, high temperatures and highly toxic chemicals are no longer required, with only water-based reaction involved. This incorporation of BGA in the production of the catalyst can mitigate the environmental impact of waste disposal while decreasing the production cost and time of the magnetic Fenton catalysts.

In this work, magnetic sugarcane bagasse ash (MBGA) can be prepared via a simple co-precipitation route using iron ions and BGA as precursors. The obtained MBGA was intensively characterized and its catalytic Fenton efficiency was analyzed for the degradation of tetracycline (TC), one of the toxic antibiotics generating problems nowadays. For the first time, we report on the use of our catalysts in degradation of TC with extremely high concentration (800 mg/L). The results indicate that nearly 100% of that TC concentration, (or degradation of 40 mg of TC) could be achieved. This value is far higher than those reported in many publications. Furthermore, our catalyst exhibited high degradation of TC even upon four cycles with excellent magnetic properties being retained. The catalysts purposed here are highly scalable.

## 2. Results and Discussion

### 2.1. Optimization of the Preparation Conditions

The raw sugarcane bagasse ash (BGA) was black, unlike the fly ash usually used as catalyst supports. The black color of BGA indicated the presence of unburned carbon particles, as confirmed by the elemental analysis. Morphological investigation using SEM on the raw BGA revealed the existence of macropores even after combustion from the sugarcane-based biomass power plant (Supplementary Materials, Figure S1). Such microporosity in BGA could allow for the facile infiltration and deposition of iron ions (both  $\text{Fe}^{2+}$  and  $\text{Fe}^{3+}$ ) into the inner pores and on the outside surfaces. Moreover, the polar-oxygenated functional groups on the BGA surface can enhance immobilization of the iron ions onto the BGA surfaces [43]. For this reason, BGA was selected as the catalyst support for this work. Upon the deposition of  $\text{Fe}^{2+}$  and  $\text{Fe}^{3+}$  ions, the addition of NaOH with heating at 80 °C can co-precipitate and transform them into magnetite ( $\text{Fe}_3\text{O}_4$ ) particles deposited on the BGA surfaces. After washing with DI water, magnetic sugarcane bagasse ash composites (MBGA) are obtained. The effects of NaOH concentration and expected  $\text{Fe}_3\text{O}_4$  to BGA ratio on the appearance and the physicochemical properties of MBGA were investigated. For the effect of NaOH concentration, all the samples (MBGA1-1, MBGA2-1, and MBGA5-1) were similarly brown-black in color (Figure S2). However, only MBGA2-1 was easily attracted by an external magnet when dispersed in DI water (Figure S3), while MBGA1-1 and MBGA5-1 showed only slight magnetic properties. For control, synthetic  $\text{Fe}_3\text{O}_4$  was glossy black and strongly attracted by a magnet. This agrees with the saturation magnetization ( $M_s$ ) from VSM analysis (Figure 1). The magnetization values for all samples were summarized in Table 1. All the investigated samples show hysteresis loops in the  $\pm 10$  kOe range at 300 K, exhibiting superparamagnetic characteristics. The  $M_s$  of MBGA1-1

was only 1.02 emu/g, which was considered almost non-magnetic and is unsuitable for practical applications. The reason for this involves the use of a low concentration of NaOH to precipitate all iron ions into the magnetic particles, according to the stoichiometric ratio in the preparation of  $\text{Fe}_3\text{O}_4$ . In contrast, MBGA2-1 possessed  $M_s$  as high as 28.71 emu/g. Table 1 shows that the yields of the prepared catalysts were quite low for MBGA1-1 and much lower for MBGA5-1. The reason for the very low yield of only 6.15% of MBGA5-1 resulted from the excessive use of NaOH, leading to the digestion of carbon and silica (the main components in the BGA) under alkali conditions [56,57]. Although the magnetic properties of MBGA5-1 were acceptable ( $M_s = 10.94$  emu/g), their lowest yield must be a problem for the real production and cost efficiency. According to the above reasons, in this study, the optimum NaOH concentration was found to be 2 M.

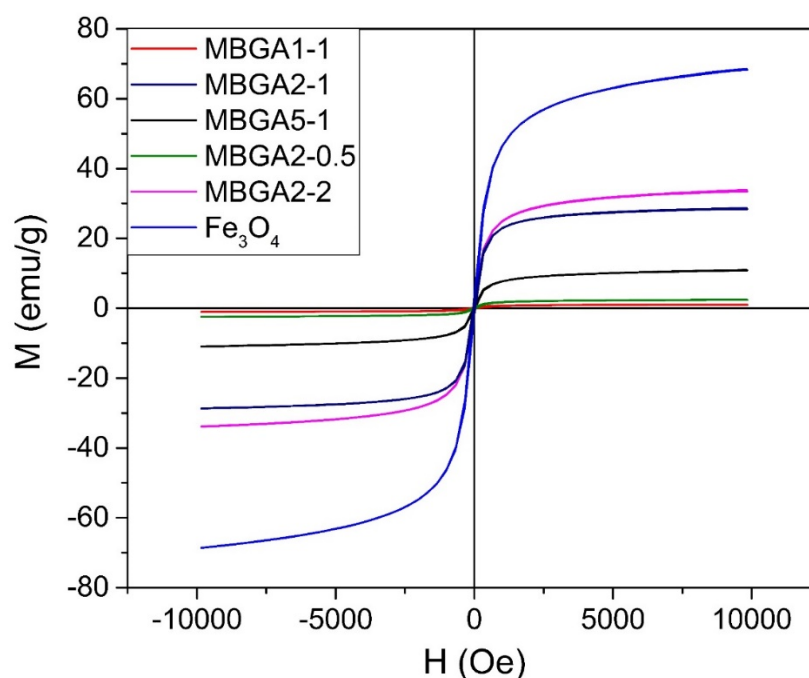


Figure 1. VSM hysteresis loops for all samples.

Table 1. Optimization of the preparation conditions and their physical and chemical properties.

Sample	NaOH (M)	Ratio of $\text{Fe}_3\text{O}_4$ /BGA	Overall Yield (%)	$M_s$ (emu/g)	%C (wt%)	pH <sub>PZC</sub>	$S_{\text{BET}}$ ( $\text{m}^2/\text{g}$ )
BGA	-	-	-	-	11.68	2.62	55.2817
$\text{Fe}_3\text{O}_4$	5	-	$53.93 \pm 3.41$	68.603	0.14	3.98	62.0286
MBGA2-0.5	2	1:2	$26.37 \pm 4.69$	2.4508	7.45	3.62	85.4644
MBGA2-1	2	1:1	$68.67 \pm 5.49$	28.705	5.53	4.14	96.0017
MBGA2-2	2	2:1	$79.94 \pm 3.91$	33.878	3.44	4.32	60.0747
MBGA1-1	1	1:1	$19.42 \pm 2.54$	1.0193	6.12	-	-
MBGA5-1	5	1:1	$6.15 \pm 2.82$	10.943	5.81	-	-

The effect of expected  $\text{Fe}_3\text{O}_4$  to BGA ratio on the physical appearances indicates that all samples (MBGA2-0.5, MBGA2-1, MBGA2-2) show the same almost-black color as others and can be attracted by a magnet (Figure S3).  $M_s$  values of this sample series were found to be correlated with the amount of the irons used.  $M_s$  values of MBGA2-1 and MBGA2-2 were similar ( $\sim 30$  emu/g), but MBGA2-2 required two times the amount of iron (Figure 1). MBGA2-0.5 showed  $M_s$  of only 2.45 emu/g due to its lowest iron sources content. Moreover, the carbon content for all samples (Table 1) confirms there was carbon left from the raw BGA, even after co-precipitation of the iron ions. This agrees with black color as a precursor for BGA and all MBGA samples.



## 2.2. Characterization of MBGA2-0.5, MBGA2-1, and MBGA2-2

To study in detail the morphology, surface chemistry, and the mechanisms for the formation of iron oxides on BGA, various intensive characterization techniques were employed.

The FESEM-EDX results for all samples (Figure S1) show macropores retained from the natural xylem and phloem of raw bagasse. This fact suggests that the combustion process in the power plant and subsequent magnetization with a co-precipitation method did not change the macropore morphology of the bagasse, implying the existence of a stable inorganic skeleton (mostly oxide compounds). These remaining macropores in BGA could be the advantage which enhances the diffusion of gigantic molecules such as TC. Besides, it is clearly seen that there were some nearly spherical silica particles in all samples. These nearly spherical particles of about  $\sim 5\text{--}30\ \mu\text{m}$  diameter originated from the combustion process of bagasse and the inorganic components were changed to oxide compounds such as  $\text{SiO}_2$ ,  $\text{CaO}$ , and  $\text{Al}_2\text{O}_3$  [55,58]. This silica–carbon composite could enhance the stability of catalyst support [59,60]. Moreover, the BGA surface was smoother than that of MBGA catalyst samples because the iron oxide particles precipitated on the BGA surface, resulting in a rough surface. Furthermore, the macropores may increase the diffusion rates of pollutants into the inner pores, while the iron oxide particles act as active sites for a heterogeneous Fenton reaction. The iron particles distributions for all samples were homogeneous, as shown in the EDX mapping (Figure S1), and the average iron content was 4.14, 9.84, and 13.70 wt% for MBGA2-0.5, MBGA2-1, and MBGA2-2, respectively. This agrees well with FESEM images, which showed that the BGA surface tended to be rougher when the iron-to-BGA ratio increased as a result of more iron oxide particles being deposited on BGA surface. Furthermore, the carbon content was decreased as this iron ratio increased, according to the trend determined by elemental analysis (Table S1). This is also confirmed by XRD patterns in Figure 2A. The XRD patterns of magnetite ( $\text{Fe}_3\text{O}_4$ , JCPDS No. 01-084-2782) and silica ( $\text{SiO}_2$ , JCPDS No. 01-070-3755) can clearly be seen. These patterns agree with the XRD of BGA and  $\text{Fe}_3\text{O}_4$  prepared with the same method but without BGA. Moreover, it is noted that MBGA2-0.5, MBGA1-1, and MBGA5-1 showed low relative intensity of the characteristic peak of magnetite at  $35.6^\circ$  (311) which agreed well with their low  $M_s$  values from VSM results.

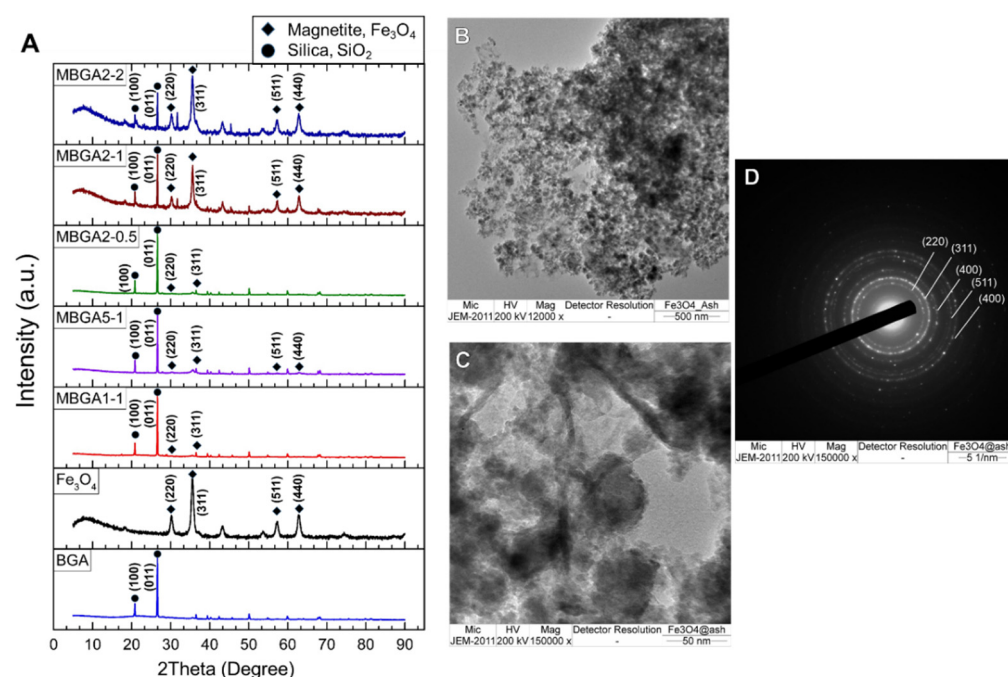


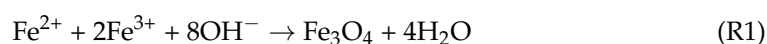
**Figure 2.** (A) XRD patterns for all samples (B,C) TEM image of MBGA2-1 at 12,000 $\times$  and 150,000 $\times$ , respectively (D) SAED pattern showing diffraction rings corresponding to  $\text{Fe}_3\text{O}_4$ .

The surface chemistry of samples was studied by FTIR spectroscopy as shown in Figure S4, and the band assignments are detailed in Table S2. The characteristic band of cellulose around  $\sim 1055\text{ cm}^{-1}$ <sup>43</sup> and considerable amounts of oxygenated functional groups of carbonaceous surface from the unburned materials were retained on the surfaces of BGA after the combustion process, which displays the absorption bands at 3435, 2924, 1631, and  $\sim 1055\text{ cm}^{-1}$ , assigned to stretching vibrations of O-H, C-H, aromatic C=C or C=O, and C-O and Si-O-Si bonds, respectively. Moreover,  $\text{pH}_{\text{PZC}}$  measured with the Zeta potential technique in Table 1 suggests that the surface of BGA and all MBGA samples was acidic. This is in agreement with the oxygenated oxidic functional groups on the BGA surface.

The similarity of the FTIR spectra and  $\text{pH}_{\text{PZC}}$  for all samples suggests that the oxygenated functional groups on the surface show no difference regarding the heterogeneous Fenton reaction. It was found that the main oxygenated functional groups of MBGA samples from C 1s and O 1s high-resolution spectra were all similar, including carboxylic, hydroxyl, and ether groups. This provides hydrophilic character, and the peak at 530 eV binding energy that corresponds to magnetite ( $\text{Fe}_3\text{O}_4$ ) [61]. The wide-scan XPS and high-resolution C 1s and O 1s spectra of MBGA2-1 were shown in Figure 3. This is consistent with the band for Fe-O bonds around  $\sim 604\text{ cm}^{-1}$  in the FTIR spectra and the magnetite pattern in the XRD results. These confirm the presence of magnetite particles on the surface of BGA. The provided detail of peak assignments for deconvoluted XPS peaks and the elemental compositions from survey scan XPS spectra of MBGA2-1 were shown in Tables S3 and S5, along with the binding energies.

To further investigate the presence of  $\text{Fe}_3\text{O}_4$  particles in MBGA2-1, TEM-EDS analysis was performed. The magnetite particles were homogeneously distributed on the BGA support as observed in the TEM images as dark spherical particles with sizes of 15–40 nm (Figure 2B,C). Furthermore, the SAED pattern for MBGA2-1 is shown in Figure 2D. The five rings obtained from the SAED image are indexed to magnetite, which agrees with the XRD results. Moreover, the EDS spectra in Figure S5 shows C, O, Fe, and Si elements distributed homogeneously all over the samples, which agree well with EDX mapping.

For the chemical equation of the preparation of MBGA using a co-precipitation method, it can be concluded that hydroxide ions react with ferrous and ferric ions as shown in reaction (R1) [17,30,62]



After that, the precipitated magnetite particles were deposited on the BGA surface, resulting in the magnetic properties of a whole sample piece. This carbon–silica support raised more chemical and mechanical stabilities of the catalyst [59,63]. Moreover, this method provides a facile single-step and scalable technique to utilize the waste precursor (BGA) as received from power plants without additional complex steps to manufacture functional catalysts.

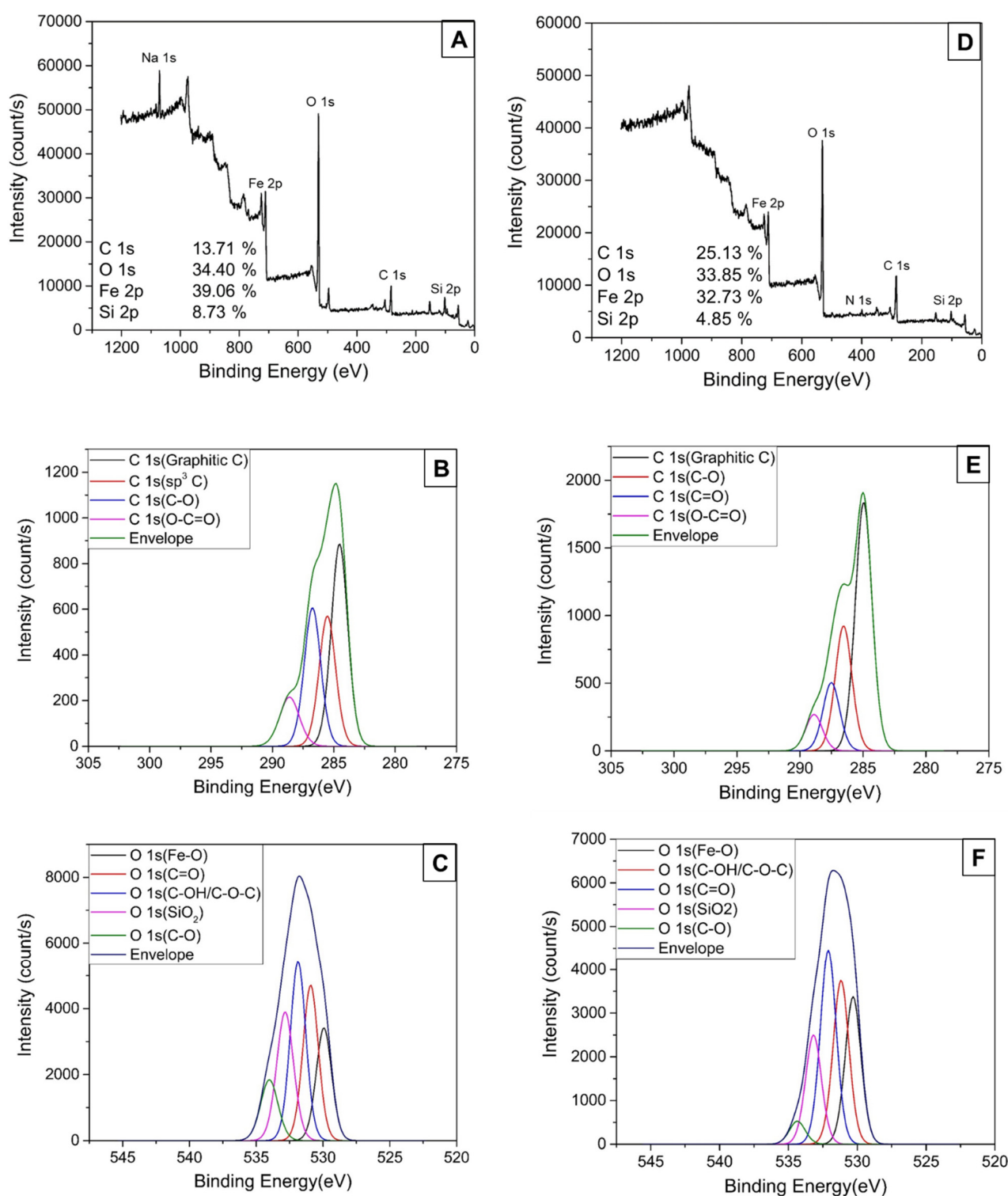


**Figure 3.** (A) The wide-scan XPS, (B,C) high-resolution C 1s and O 1s spectra of fresh MBGA2-1 (D) The wide-scan XPS, (E,F) high-resolution C 1s and O 1s spectra of MBGA2-1 after 4 cycles using 0.1 M NaOH as eluent.

### 2.3. Preliminary Catalytic Heterogeneous Fenton Reaction Test of Magnetic Sugarcane Bagasse Ash

To study the possibilities of the MBGA samples as the heterogeneous Fenton catalyst, the catalytic degradation test of tetracycline (TC) was investigated. The reaction was started by adding 5 mM of  $H_2O_2$  into the 50 mL of 800 mg/L TC solution at natural pH (pH 3.2) with a catalyst concentration of 1 g/L. The result, as shown in Figure S6A, suggests

that MBGA2-1 and MBGA2-2 have similar removal efficiency for TC after 12 h reaction time; around ~90%. Even the iron content in MBGA2-2 was higher, while the removal efficiency for MBGA2-0.5 was slightly lower due to a lower iron amount on the surface of the catalyst. For control, only TC degraded with 5 mM of H<sub>2</sub>O<sub>2</sub> without a catalyst was also studied, and only 12.56% of TC was degraded. Furthermore, pure Fe<sub>3</sub>O<sub>4</sub> (ground into power with the particle size of ~50 µm) revealed only 47.66% removal. This confirms that use of BGA as a catalyst support can significantly increase the removal efficiency. Furthermore, the Fe leaching tests for all samples showed that MBGA2-2 had the highest Fe leaching of 4.58 mg/L, while it was only 0.61 and 0.28 mg/L for MBGA2-1 and MBGA2-0.5, respectively. The high leaching of iron from MBGA2-2 was due to the excess amount of iron precursors which could not strongly attach to the surface of catalyst support and could easily be dissolved in natural acidic TC solution. When taking BET surface area into consideration, as shown in Table 1, as is known to all, the high BET specific surface area is beneficial for more guest molecules to access active sites. The MBGA2-1 also showed the highest BET surface area of 96 m<sup>2</sup>/g. According to all information and intensive characterization techniques, MBGA2-1 was selected as a promising Fenton catalyst for the catalytic degradation of TC because of the high removal efficiency with low Fe leaching, and high stabilities with strong magnetic properties. Moreover, it also has the highest BET surface area and suitable surface characters with low-cost preparation. For the effect of catalyst concentration, as shown in Figure S6B, the degradation efficiency increased with increasing catalyst loading. Therefore, it was fixed at 1 g/L for all other experiments because it was the minimum amount of the catalyst which can be a representative for the whole sample in the catalytic degradation experiments. This can be considered by the standard deviation, in which 1 g/L shows the lowest value with ~90% efficiency, while 2 g/L shows only 5% higher efficiency but uses double the amount of catalyst.

#### 2.4. Catalytic Degradation of TC by MBGA2-1: Effect of pH

Generally, solution pH can significantly influence the catalytic degradation in the Fenton system [10,64]. The effect of pH on the catalytic degradation of TC by MBGA2-1 was investigated. The experiment was conducted as shown in Figure 4A. The studied pH solution was 3.2 (natural pH), 5, 7, 9. The natural pH at 3.2 showed the highest removal efficiency of 90.43% for MBGA2-1. It is worth noting that when pH is higher, the efficiency decreased due to the reduced reactivity of radicals and the precipitation of iron ions [10]. Furthermore, MBGA2-1 shows over two times greater removal efficiency than pure Fe<sub>3</sub>O<sub>4</sub>, again confirming the advantage of BGA as catalyst support. In absence of the catalyst, H<sub>2</sub>O<sub>2</sub> alone in natural pH can degrade TC with only ~14%. In addition, 6 h is the equilibrium time for all samples in this catalytic degradation of 800 mg/L TC solution. Therefore, the unadjusted natural pH (3.2) was chosen to be the optimum pH for further experiments.

To evaluate the kinetics of TC catalytic degradation, the data were fitted with a linear pseudo-first-order model shown as Equation (1):

$$\ln C_t = -k_1 t + \ln C_0 \quad (1)$$

where  $k_1$  is a rate constant for catalytic degradation in the pseudo-first-order model, and  $C_t$  is the TC concentration at time  $t$ . The kinetics of the adsorption-co-catalytic degradation of the MBGA samples were fitted well with pseudo-first-order reaction with good R<sup>2</sup> and the calculated pseudo-first-order rate constants, as shown in Figure S7. On the other hand, under basic conditions, the degradation rate decreased, and the removal efficiencies at pH 7 and 9 were almost the same. Moreover, it is noted that the pseudo rate constant of the MBGA2-1 at natural pH was 0.1047 h<sup>-1</sup>, which was 2.3 and nearly 4 times higher than pH 5 and pH 7, respectively. This is due to Fenton reactions being favored under acidic conditions.



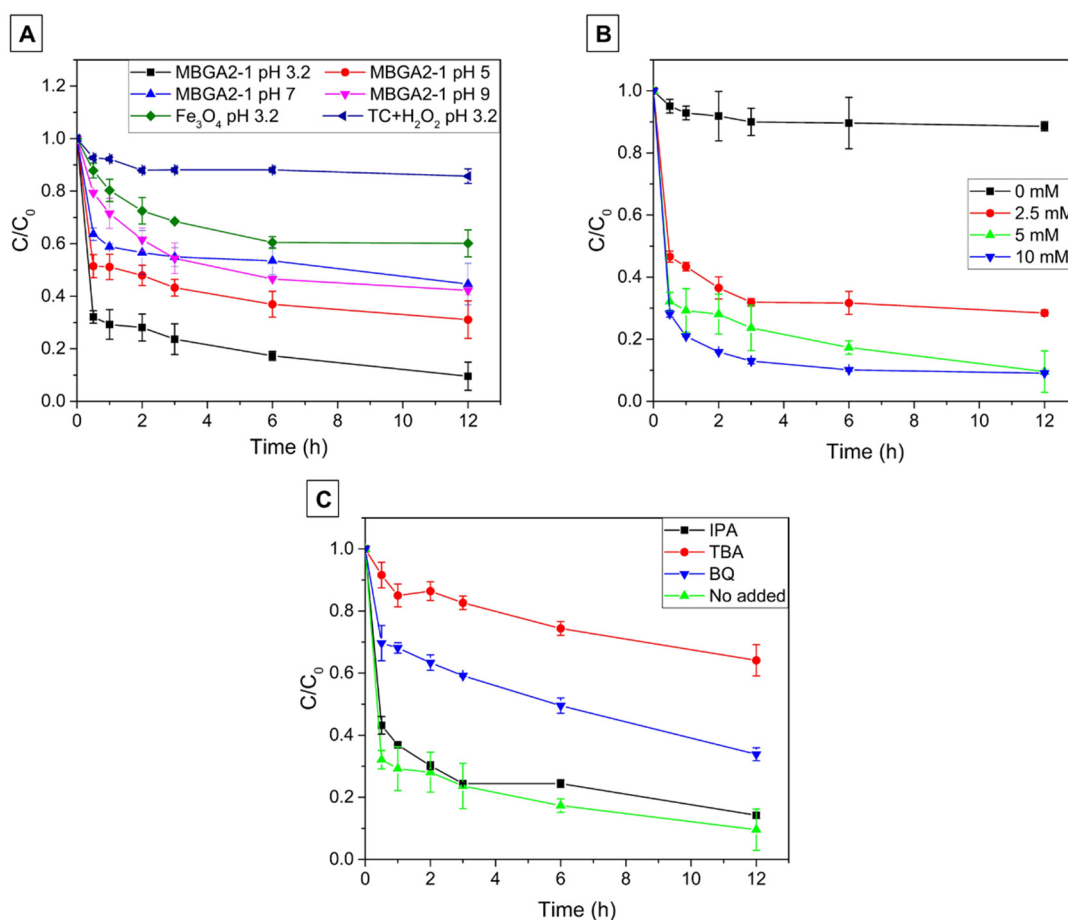


**Figure 4.** The catalytic degradation of TC (A) Effect of pH (B) Effect of  $H_2O_2$  concentration (C) Effect of scavenger (conditions:  $C_0 = 800$  mg/L, pH 3.2 (natural),  $H_2O_2$  concentration = 5 mM, catalyst concentration = 1 g/L,  $T = 28 \pm 2$  °C).

### 2.5. Catalytic Degradation of TC by MBGA2-1: Effect of $H_2O_2$ Concentration

To investigate the effect of  $H_2O_2$  concentration on the catalytic degradation of TC, the experiments with different  $H_2O_2$  concentrations (0, 2.5, 5, 10 mM) were conducted as shown in Figure 4B. In absence of the  $H_2O_2$ , the adsorption of MBGA2-1 alone can remove only 11.4% of TC (actual adsorption capacity of 90.32 mg/g) due to the limited adsorption sites. Note that even without addition of  $H_2O_2$ , the removal of TC could reach up to 90 mg/g due to the pure adsorption mechanism. This strongly suggests the importance of using BGA as a catalyst support because of the ability of the carbon left from combustion process to attract the TC molecules. The removal efficiency for MBGA2-1 increased with the increasing  $H_2O_2$  concentration. The removal efficiency can reach up to 80% at 6 h for 5 mM  $H_2O_2$  concentrations. Nevertheless, while the  $H_2O_2$  dosage rose from 5 to 10 mM, the removal efficiency barely increased, and the same efficiencies were reached at 12 h. This is because the excess  $H_2O_2$  can compete with TC for  $\cdot OH$  as shown in reaction (R2–R3) [64].



Even though 10 mM shows the highest rate in the first few hours, the same efficiencies were reached at 12 h. Therefore, to minimize the cost of operation, 5 mM of  $H_2O_2$  was selected as the optimum concentration.

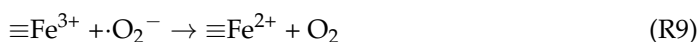
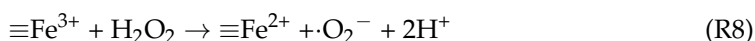
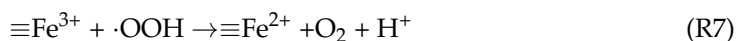
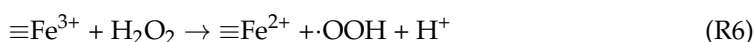
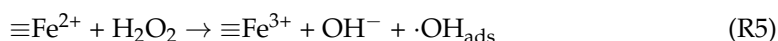
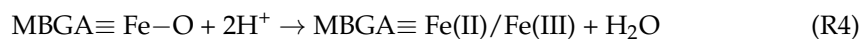
## 2.6. Catalytic Degradation of TC by MBGA2-1: Effect of Scavenger and Its Mechanism

To identify free radicals in Fenton oxidation experiments, different types of free-radical-trapping agents were added into the reaction systems to identify the difference of contributions to the degradation efficiency between different free radicals. In this experiment, 0.3 M tert-butyl alcohol (TBA) was used as a hydroxyl radical ( $\cdot\text{OH}$ ) scavenger, while 20 mM p-benzoquinone (BQ) was used as a superoxide radical ( $\cdot\text{O}_2^-$ ) scavenger [65,66]. As shown in Figure 4C, the introduction of TBA remarkably inhibited TC degradation and the removal efficiency was only 35.87% at 12 h, while adding 20 mM BQ caused a slight drop in the degradation efficiency from 90.43% without scavenger to 66.13% at 12 h. This demonstrated that  $\cdot\text{OH}$  was the major reactive oxygen species in this heterogeneous Fenton system.

To explain the mechanisms of the AOP by  $\cdot\text{OH}$  radicals in detail, two types of hydroxyl radicals were used to distinguish them. First, 0.3 M isopropanol (IPA) was utilized to individually trap free hydroxyl radicals ( $\cdot\text{OH}_{\text{free}}$ ), while it was well known that TBA could quench both free  $\cdot\text{OH}$  in solution ( $\cdot\text{OH}_{\text{free}}$ ) and  $\cdot\text{OH}$  adsorbed onto the surface of a catalyst ( $\cdot\text{OH}_{\text{ads}}$ ) [65,66]. Notably, the addition of IPA slightly suppressed the degradation of TC and the removal efficiency showed only a 4.65% drop at 12 h, indicating that only a low amount of  $\cdot\text{OH}_{\text{free}}$  was present in the system. Moreover, it can be concluded that  $\cdot\text{OH}_{\text{free}}$ ,  $\cdot\text{OH}_{\text{ads}}$ , and  $\cdot\text{O}_2^-$  contributed to the degradation of TC by a heterogeneous Fenton system. However,  $\cdot\text{OH}_{\text{ads}}$  on the MBGA2-1 surface was the only major reactive species responsible for the catalytic degradation of TC.

To confirm that the major mechanisms of the removal of TC mainly involved catalytic degradation rather than adsorption, the total organic carbon (TOC) of the solution before and after the catalytic degradation of TC was determined, and the TOC removal was 56.70%, indicating that a huge amount of TC in the solution was transformed into inorganic compounds ( $\text{CO}_2$  and  $\text{H}_2\text{O}$ ). Moreover, the dramatic decrease in peak at  $m/z$  at 443.15 after the complete catalytic degradation of TC analyzed by LC-MS in Figure S8 suggests that the intermediates generated from the Fenton system were quickly oxidized into inorganic compounds. It is worth noting that the low TOC after catalytic testing also suggests that the BGA as a support released no organic compounds, unlike the release of polyaromatic hydrocarbon molecules (PAHs) in aqueous systems from various solids obtained through the combustion process. This further confirms the chemical stability of the support in this work and could eliminate the concern over the toxic chemicals released from the BGA.

The catalytic mechanism of  $\text{H}_2\text{O}_2$  via MBGA2-1 composite is proposed in Figure 5. Firstly, the surface of the MBGA2-1 will rapidly form iron ions under acidic conditions as shown in (R4), then the surface of catalyst was adsorbed by  $\text{H}_2\text{O}_2$ , and it was quickly decomposed to  $\cdot\text{OH}_{\text{ads}}$  by the Fe(II) on the surface of MBGA2-1, as shown in reaction (R5), while Fe(III) on the surface can react with  $\text{H}_2\text{O}_2$  to generate perhydroxyl radicals ( $\cdot\text{OOH}$ ) or superoxide radicals, and the regeneration of Fe(II) by the reduction of Fe(III) can continue the catalytic cycle (R6–R9) [11,67,68].



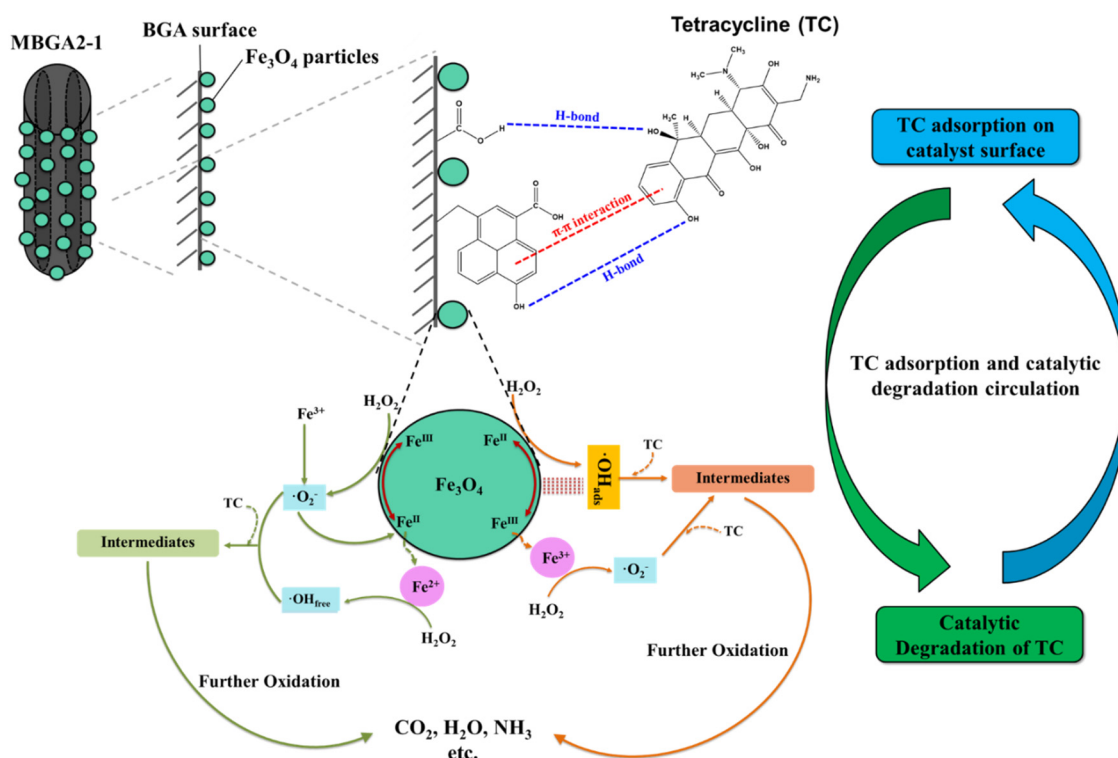


Figure 5. The TC catalytic degradation mechanism.

However, the dissolution of iron ions in the solution was inevitable due to the acidity of the solution, and the deposition of iron particles was on the surface of BGA, not in the carbon matrix. Hence, the same mechanism mentioned above also occurred to generate a little amount of  $\cdot\text{OH}_{\text{free}}$  indicating the low Fe leaching in the solution. Moreover, the presence of ferrous ions from  $\text{Fe}_3\text{O}_4$  on the surface of catalyst is especially favored under acidic conditions, and they played the most important role in the formation of  $\cdot\text{OH}_{\text{ads}}$  in the reaction, which was the main reactive oxygen species.

## 2.7. Catalytic Degradation of TC by MBGA2-1: Effect of TC Concentration

The effect of TC concentration on TC degradation is presented in Figure 6. It was observed that the initial rate of degradation increased with the increase in the initial concentration of TC, but it barely increased when the initial TC concentrations were higher than 800 mg/L, indicating that the active sites of catalyst were occupied by TC molecules, and TC molecules cannot access the active sites at higher concentrations. This was confirmed by the removal efficiencies at 12 h, at which the high initial concentrations of TC showed lower efficiencies. Moreover, the removal capacity ( $Q_e$ ) also increased with the increased initial TC concentration.

Furthermore, it is known that any heterogeneous reaction, as in the case of a Fenton reaction, is highly affected by the interactions between pollutant molecules and catalysts, including two consecutive steps. Firstly, the reactant molecules are adsorbed on the surface of the catalyst and followed by immediate degradation. To confirm this mechanism, the Langmuir–Hinshelwood equation was applied for MBGA2-1 as shown in the inset of Figure 6, and the linear expression of the Langmuir–Hinshelwood plot was as follows [69]:

$$\frac{1}{v_0} = \frac{1}{kK_{\text{ads}}C_0} - \frac{1}{k} \quad (2)$$

where  $v_0$  is the initial rate of TC degradation, mg/L·s;  $k$  is reaction rate constant, mg/L·s, and  $K_{\text{ads}}$  is the Langmuir–Hinshelwood adsorption equilibrium constant, L/mg. The good fitness of the Langmuir–Hinshelwood equation with  $R^2$  of 0.9974 confirmed the above

assumption and also agreed with the mechanism where  $\cdot\text{OH}_{\text{ads}}$  played the main role as the reactive oxygen species for TC degradation. The rate constant and adsorption equilibrium constant were reported in Table S5.

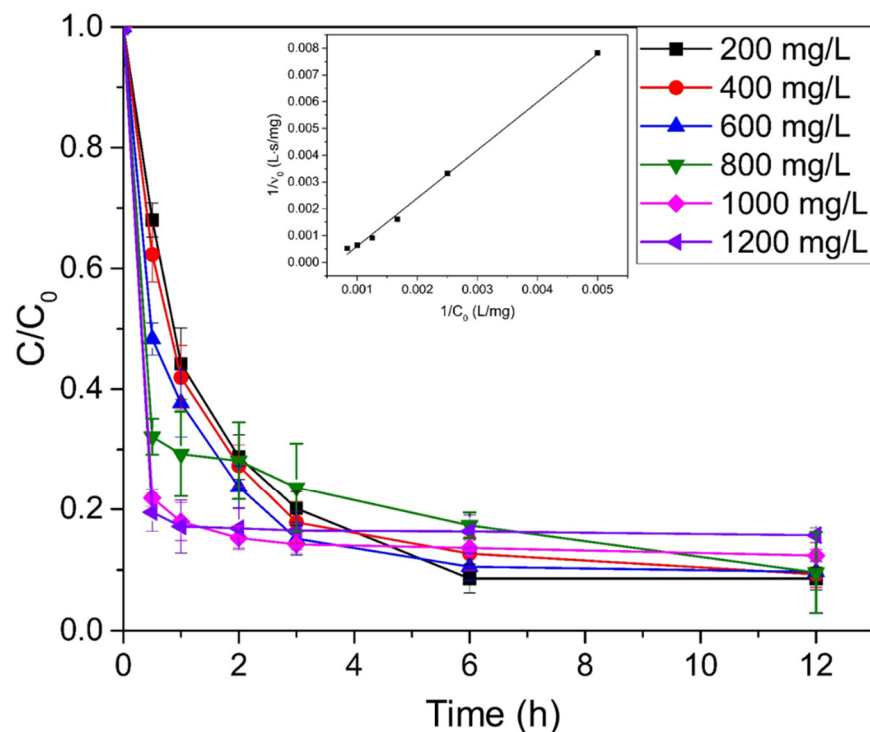


**Figure 6.** Effect of initial TC concentration on the catalytic degradation of TC and (inset) the Langmuir–Hinshelwood (L-H) plot (conditions:  $C_0 = 200\text{--}1200$  mg/L, pH 3.2 (natural),  $\text{H}_2\text{O}_2$  concentration = 5 mM, catalyst concentration = 1 g/L,  $T = 28 \pm 2$  °C).

The agreement of this model assumption with data indicates the important role of the silica–carbon support, which not only had high chemical stability but also enhanced TC adsorption by H-bond and  $\pi$ – $\pi$  stacking, leading to the increase in the Fenton reaction’s efficiency [43,60,70,71]. It could be proposed that after TC molecules were adsorbed on the surface of catalyst, the catalytic degradation of TC occurred and degraded to inorganic products, then the new incoming TC molecules adsorbed again on the surface of catalyst, creating the circulation as also shown in Figure 5. This could explain why this catalyst was able to degrade the high amount of TC almost completely in the solution (800 ppm TC).

Moreover, the TC level in real wastewater is generally low [72]. It is interesting to note that all 40 mg/L TC in 50 mL solution was removed and could not be measured by UV-Vis spectrophotometer. Therefore, 1000 mL of 40 ppm TC solution with the same amount of TC molecules compared to 50 mL of 800 ppm TC was used in the catalytic experiment with the same conditions as before. The result in Figure S9 indicates a removal efficiency of 85.47% which was only 5% lower than the catalytic degradation of 800 ppm TC with the volume of 50 mL. This was because the natural pH of lower concentration of TC (40 ppm) slightly increased (pH 4.4), leading to the decrease in the catalytic activity of the heterogeneous Fenton reaction [10], and the lower initial concentration of the reactant (TC) can decrease the initial reaction rate, according to the principles of rate law. Furthermore, the high reaction volume can also slow down the reaction in which the catalyst has limited active sites to be in contact with pollutant molecules. Moreover, the comparison studies were also investigated, as shown in Figure S10. The adsorption process in dark conditions was first carried out for 3 h to ensure that the TC molecules were fully adsorbed by the catalyst, then the Fenton reaction started with the addition of  $\text{H}_2\text{O}_2$ . The results showed that the similar removal efficiency was obtained for the first 3 h compared to the experiments without

H<sub>2</sub>O<sub>2</sub> in Figure 4B. Finally, the removal efficiency after 12 h was achieved at 90.24%, which was very close to the prior experiment in the same conditions, but the H<sub>2</sub>O<sub>2</sub> and catalyst were added into TC solution simultaneously. This confirms that there is no significant difference in the final efficiencies between both experiments.

## 2.8. The Regeneration of MBGA2-1

The recyclability of the catalyst is a crucial criterion for evaluating its practicability. The catalytic degradation experiment of 800 ppm TC (50 mL) with MBGA2-1 was first conducted using 5 mM H<sub>2</sub>O<sub>2</sub> at natural pH. After that, the catalyst was regenerated by using DI water and 0.1 M NaOH as eluting agents. As shown in Figure 7A, the initial degradation efficiency of MBGA2-1 was 90%. After four regeneration cycles with NaOH and DI water as the eluents, the degradation efficiencies of MBGA2-1 were dropped to 68.97% and 37.86%, respectively. The results show that the recyclability of the catalyst was acceptable, with high efficiency in removal of TC. Additionally, 0.1 M NaOH was also found to be a better eluent than DI water. More importantly, some of TC was detected by UV-vis spectrophotometer from the eluate, confirming that simple adsorption also contributes to the TC removal. This was consistent with the elemental composition from the XPS result in Table S4. It was found that after regeneration for four cycles, MBGA2-1 had 1.73% wt nitrogen content, while it was not found on fresh MBGA2-1. Moreover, it was found that NaOH is a great eluent for TC on carbon materials, leading to better recyclability [43,73–75]. The alkaline solution can make the catalyst surface become more basic and can suppress the iron dissolution, as confirmed in Figure 7B. The iron leaching for each cycle using both DI water and 0.1 M NaOH as eluents shows the remarkable low Fe leaching in range of 0.2–0.8 mg/L when using NaOH as an eluting agent, which was lower than the EU discharge standards (<2 mg/L) [15] and also consistent with the recyclability results. Furthermore, the used MBGA2-1 was also characterized by high-resolution XPS and VSM analysis, as shown in Figure 3D–F and Figure S11. The surface chemistry based on C 1s and O 1s (Table S3) of used MBGA2-1 was found to be the similar to that of fresh MBGA2-1, while the iron content dropped insignificantly (Table S4), and the saturation magnetization of used MBGA2-1 slightly decreased. Although the M<sub>s</sub> decreased for used MBGA2-1, the value was considered high, and the catalyst could still strongly be attracted by an external magnet. This proved that the catalyst developed in this work is stable.

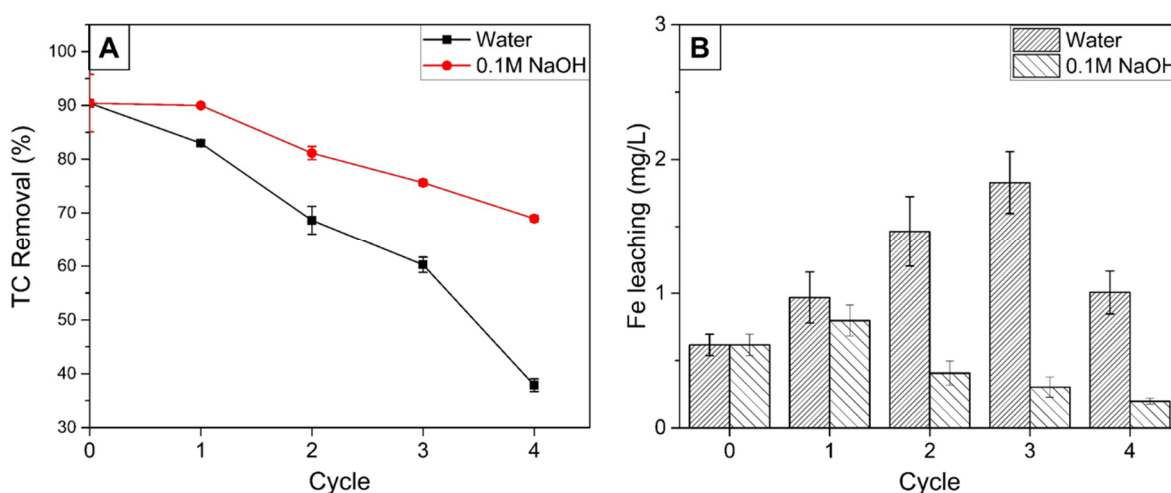


**Figure 7.** (A) The recycled experiments with different eluting agents; (B) the iron leaching after the degradation experiments for each cycle (conditions:  $C_0 = 800$  mg/L, pH 3.2 (natural), H<sub>2</sub>O<sub>2</sub> concentration = 5 mM, catalyst concentration = 1 g/L,  $T = 28 \pm 2$  °C).



### 2.9. Comparison Studies

In order to justify the MBGA2-1 as a good Fenton catalyst for the catalytic degradation of TC, a comparison with previously published studies is shown in Table S6. The magnetic Fenton catalyst in this work prepared using a simple co-precipitation method used low toxic chemicals in water-based reaction. In contrast, others previous works have employed complicated steps and large amount of chemicals, including the preparation of supports themselves. The use of such synthetic catalyst supports has also led to difficulty in scaling up, burdening the practical uses. Furthermore, in some works, toxic metals were introduced to accelerate the Fenton cycle, leading to secondary contamination with the remaining, highly toxic metals. In the present work, the utilization of Fe alone as active metal renders the easily scalable application to pilot scale in industries because the Fe precursor is relatively low cost, abundant, and non-toxic. With our catalyst, at 3 h, the removal efficiency increased rapidly to 78%, and up to 90% within 12 h. In terms of the removal efficiency, the removal amount of TC per catalyst dosage ( $Q_c$ ) was calculated and normalized to compare the performance of TC degradation due to differences in initial TC concentration and reaction volume from various works. Although the pseudo-rate constant of MBGA2-1 was lower compared to those of other catalysts, our catalyst showed the highest  $Q_c$  of 721.32 mg/g among similar catalysts, both using a Fenton system and a photocatalytic system. This value is considered to be extremely high. To the best of our knowledge, its removal amount of TC per catalyst dosage ( $Q_c$ ) was the highest among all of the Fenton catalysts so far. Moreover, the  $H_2O_2$  concentration used in this work was considered low, and only a simple Fenton process is needed without the requirement of visible, UV light, or ultrasound, leading to cost-effectiveness in a real operation. In addition, the catalyst can easily be recovered from the solution by an external magnet after the process. Therefore, this MBGA2-1 is a promising Fenton catalyst to apply in practical industrial applications.

## 3. Experimental Section

### 3.1. Materials

Ferrous sulfate heptahydrate ( $FeSO_4 \cdot 7H_2O$ , 99.5%) was purchased from Sigma-Aldrich (Burlington, MA, USA), Ferric Chloride Hexahydrate ( $FeCl_3 \cdot 6H_2O$ , 99.0%) was purchased from Loba Chemie (Colaba, Mumbai). NaOH (97.0%) was purchased from RCI Labscan. HCl (36.5–38.0%) was purchased from J.T. Baker (Phillipsburg, NJ, USA). Tetracycline Hydrochloride (TC·HCl, >98.0%) was purchased from TCI America (Portland, OR, USA). Sugarcane bagasse ash (BGA) was obtained from sugar plant of Eastern Sugar and Cane Public Company Limited (Sa Kaeo, Thailand) and was thoroughly washed to remove dirt and used as catalyst support without any further purification. All experiments were performed using deionized (DI) water and all chemicals were AR grade.

### 3.2. Characterization of Samples

Field Emission Scanning Electron Microscope with energy dispersive X-ray spectroscopy (FESEM-EDX, Apreo, FEI, Brno-Černovice, Czech Republic) was operated to study surface and porous morphology and magnetic particles. Fourier transform infrared spectroscopy (FT-IR, Spectrum GX, Perkin Elmer, Waltham, MA, USA) with a KBr pellets technique in wavenumber ranges of  $4000\text{--}400\text{ cm}^{-1}$  and X-ray photoelectron spectroscopy (XPS, AXIS Ultra DLD, Kratos Analytical Ltd., Manchester, UK) were performed to determine functional groups and iron species on the surface, both quantitatively and qualitatively.  $N_2$  adsorption–desorption isotherms (ASAP2460, Micromeritics, Norcross, GA, USA) were used to determine specific surface area. The samples were degassed at  $120\text{ }^\circ\text{C}$  for 16 h prior to the measurements. X-ray Powder Diffraction (XRD, Philips, X'Pert MPD, Almelo, The Netherlands) was performed to study crystal structure and the form of iron in samples. The scan was run from  $5^\circ$  to  $90^\circ$  with a step size of  $0.05^\circ$ . A vibrating sample magnetometer (VSM, Lakeshore, Westerville, OH, USA) was used to study magnetic properties of samples at 298 K. Transmission electron microscopy with Energy Dispersive Spectroscopy (TEM-EDS, JEOL JEM-2010, Tokyo, Japan) was operated at 200 kV to study the uniformity

of distribution, sizes, and other characteristics of the magnetic particles. Zeta potential (Zeta Potential Analyzer, ZetaPALS, Brookhaven, Holtsville, NY, USA) was performed to evaluate the point of zero charge ( $pH_{PZC}$ ) to study the acid base or total charge on the surface of samples. The stability of the magnetic composite was studied by collecting the composite after the reaction under different conditions. After that, the total number of Fe ions left in the solution was measured by ICP-OES (AVIO 500, Perkin Elmer, Waltham, MA, USA) to confirm the iron leaching from the composite. The solution after the experiments was measured using a UV-Vis spectrophotometer and liquid chromatography-mass spectra (ESI<sup>+</sup> mode, Agilent Technologies, Santa Clara, CA, USA). The decay of the total organic carbon (TOC) in the solution was also evaluated by TOC analyzer (multi N/C 3100, Analytik jena, Jena, Germany).

### 3.3. Preparation of Magnetic $Fe_3O_4$ @ash Composite

Magnetic carbon materials were synthesized by the following steps.  $FeSO_4 \cdot 7H_2O$  and  $FeCl_3 \cdot 6H_2O$  in 1:2 mol ratio were separately dissolved in 200 mL of DI water. Then, 5.00 g sugarcane bagasse ash (BGA) with the particle size of 50  $\mu m$  was added and the mixture was stirred at 200 rpm and 80 °C in a magnetic stirring water bath. When the temperature reached 80 °C, 100 mL of 1, 2, or 5 M NaOH was added dropwise into the suspensions, then the mixture was aged for 3 h at 80 °C. After the suspensions were cooled down to RT, they were washed with DI water until the pH was ~7. Next, the magnetic solid was separated with an external magnet, then dried at 110 °C for 3 h. The magnetic sugarcane bagasse ash composite (MBGA) was obtained. The impregnation ratios of  $Fe_3O_4$ /BGA were 1:1, 2:1, and 1:2, varying the amount of iron precursor. The samples were designated with the labeling type MBGAx-y, where x represents the concentration of NaOH in M, y is the scaled ratio of  $Fe_3O_4$ /BGA; y = 1 for  $Fe_3O_4$ /BGA = 1:1; y = 0.5 for  $Fe_3O_4$ /BGA = 1:2; and y = 2 for  $Fe_3O_4$ /BGA = 2:1. For comparison,  $Fe_3O_4$  was also prepared as a control experiment with the same ratio and under the same conditions as MBGA5-1 but without the BGA. All the prepared materials were ground to ~100  $\mu m$  particle size (as determined by FESEM) before further experiments or characterization. The preparation of all samples was replicated 5 times and standard errors are reported in Table 1.

### 3.4. Experimental Procedure

**Kinetics:** The batch kinetics experiments were performed in 100 mL conical flasks with 0.05 g of the magnetic catalyst (particle size of ~100  $\mu m$ ) and 100 mL of 800 mg/L TC solution, on a thermostat shaker water bath (Model TOL09-FTSH-01, SCIFINETECH) at  $28 \pm 2$  °C, at the natural (unadjusted) pH 3.2, for 0–12 h durations.

A certain amount of  $H_2O_2$  was added to trigger the catalytic reaction and the pH was adjusted with 0.1 M HCl or 0.1 M NaOH while investigating effect of pH on the tetracycline removal.

To study the effect of TC concentration on the TC removal efficiency, the Fenton catalytic degradation experiments were performed in 100 mL conical flasks with 0.05 g of magnetic carbon material and 50 mL of 0–1200 mg/L TC solutions. The mixture was shaken for 12 h in the thermostat shaker water bath at  $28 \pm 2$  °C, at the natural pH 3.2.

All the experiments were carried out under dark conditions. After complete reaction, the solution was removed while the composite was separated from the mixture using a magnet. The concentrations of TC before and after Fenton reaction were measured by a calibrated method, using a UV-Vis spectrophotometer (UV 2600, Shimadzu, Kyoto, Japan) at  $\lambda = 357$  nm. The removal amount of TC ( $Q_e$ ) was calculated with the following equation (Equation (3))

$$Q_e = \frac{(C_0 - C_e)V}{m} \quad (3)$$

where  $C_0$  and  $C_e$  are the initial and equilibrium concentrations of TC (mg/L), respectively, m is mass of the composite (g), and V is volume of the reaction solution (L).

The degradation efficiency was calculated by the following formula (Equation (4))

$$\% \text{Efficiency} = \frac{(C_0 - C_t)}{C_0} \times 100 \quad (4)$$

where  $C_t$  are the concentrations of TC at desired time intervals (mg/L)

**Catalyst regeneration:** The recyclability of the catalyst was performed with MBGA2-1, 50 mL of 800 mg/L TC solution for 24 h on the thermostat shaker water bath at  $28 \pm 2$  °C and natural pH (pH 3.2). The concentration of  $\text{H}_2\text{O}_2$  added in the mixture was 5 mM. The composite was then collected by an external magnet. The adsorbed TC molecules were eluted from the composite by stirring the 0.5 g of the used composite in 50 mL of 0.1 M NaOH at 200 rpm for 30 min, and the eluted composite was washed with DI water until neutral pH was obtained. For comparison, the eluting agent was changed to DI water as a control. Then, the composite was dried at 110 °C for 3 h. The adsorbent was subjected to 4 consecutive experiment cycles with the same volume and concentration as the first cycle. It is noted that there was no color release observed from the composite.

#### 4. Conclusions

Magnetic  $\text{Fe}_3\text{O}_4$ @ash composites were successfully prepared with a simple co-precipitation method using low-cost sugarcane bagasse ash received as it was from the biomass electricity-generation plants. The preparation protocol and characterization were systematically studied with various techniques. The developed catalyst was used for catalytic degradation of an ultra-high concentration of TC (800 ppm) using a Fenton system. The catalytic performance showed that the MBGA2-1 catalyst had the highest degradation activity, with good magnetic properties and high stabilities, compared to pure  $\text{Fe}_3\text{O}_4$  and other samples. It was discovered that the carbon left on the surface of the ash helped attract TC molecules, enabling enhancement of the catalytic degradation process. The catalyst also had good recyclability with low Fe leaching using 0.1 M NaOH as the eluent. Moreover, the removal mechanism included two steps, starting with the TC adsorption on the catalyst support with oxygenated functionalities. After that,  $\cdot\text{OH}_{\text{ads}}$ —which was the main reactive oxygen species—attacked the molecules, leading to the degradation of TC. Additionally, we developed a new potential approach for the utilization of low-cost BGA with the circular economy concept. Considering its catalytic performance, magnetic properties, stabilities, and easily scalable preparation, the MBGA2-1 has great potential for a practical application with sustainability in wastewater remediation.

**Supplementary Materials:** The following supporting information can be downloaded at: <https://www.mdpi.com/article/10.3390/catal12040446/s1>, Figure S1: FESEM-EDX analysis; Figure S2: Physical images of all samples; Figure S3: Physical image of magnetic separation; Figure S4: FTIR spectra for all samples; Figure S5: (A) TEM image in electron mode (B-E) EDS mapping of C, O, Fe, Si, respectively; Figure S6: (A) Preliminary Catalytic Heterogeneous Fenton Reaction Test with Fe leaching for each samples, (B) The effect of catalyst concentration on the catalytic degradation of TC for MBGA2-1; Figure S7: Linear pseudo-first-order kinetics model for the catalytic degradation of TC for MBGA2-1 under different pH; Figure S8: LC-MS of the TC solution before- and after- catalytic degradation by MBGA2-1; Figure S9: Comparative studies of the catalytic degradation of low concentration of TC for MBGA2-1; Figure S10: The catalytic degradation of TC for MBGA2-1. The Fenton reaction starting by the addition of  $\text{H}_2\text{O}_2$  after the adsorption process in dark condition for 3 h; Figure S11: VSM hysteresis loop of (black) fresh MBGA2-1, and MBGA2-1 after used 4 cycles by using (red) water and (blue) 0.1M NaOH as eluents; Table S1: The elemental compositions obtained from EDX spectra; Table S2: Assignment of the peaks in FTIR spectra for all samples; Table S3: Assignment of the peaks in XPS results (C 1s and O 1s) for MBGA2-1; Table S4: The elemental compositions (in wt%) for all samples, as obtained from XPS results; Table S5: Fitted parameters in the Langmuir-Hinshelwood model; Table S6: Literature curated data on the catalyst for TC removal and results from the current studies.

**Author Contributions:** N.R.: Formal analysis, writing—original draft, designed the experiments, conducted the experiments, data analysis, drafted the manuscript, prepared the manuscript, revised the manuscript. O.D.: Formal analysis, conducted experiments, data analysis; D.D.: proofread the manuscript, provided conceptual ideas; W.W.: proofread the manuscript, provided conceptual ideas; J.P.: proofread the manuscript; S.K.: performed TEM measurements and analysis; L.C.: Formal analysis, writing—original draft, designed the experiments, conducted the experiments, data analysis, drafted the manuscript, prepared the manuscript, revised the manuscript, funding acquisition, supervision for the whole project, corresponding author. All authors have read and agreed to the published version of the manuscript.

**Funding:** This work was funded by Development and Promotion of Science Technology Talents; (DPST) Research Grant (Grant No. 017/2559 and partially supported by 2021 TTSTF Science & Technology Research Grant (Thailand Toray Science Foundation) for L. Chuenchom. N. Rattanachueskul thanks the Graduate School, Prince of Songkla University, for PSU-PhD. scholarship (Contract No. PSU\_PHD2562-003); Partial financial support from the Research Team Promotion grant—National Research Council of Thailand (Joongjai Panpranot) is acknowledged.

**Data Availability Statement:** All data are available from the corresponding author on reasonable request.

**Acknowledgments:** L. Chuenchom. would like to acknowledge the partial support from the Center of Excellence for Innovation in Chemistry (PERCH-CIC), Ministry of Higher Education, Science, Research, and Innovation. S. Kaowphong would like to thank Chiang Mai University. We thank Titilope John Jayeoye for English proofreading.

**Conflicts of Interest:** The authors declare no conflict of interest.

## References

- Wang, J.; Zhuan, R. Degradation of antibiotics by advanced oxidation processes: An overview. *Sci. Total Environ.* **2020**, *701*, 135023. [\[CrossRef\]](#) [\[PubMed\]](#)
- Zhang, Y.; Shi, J.; Xu, Z.; Chen, Y.; Song, D. Degradation of tetracycline in a schorl/H<sub>2</sub>O<sub>2</sub> system: Proposed mechanism and intermediates. *Chemosphere* **2018**, *202*, 661–668. [\[CrossRef\]](#) [\[PubMed\]](#)
- Xiang, Y.; Huang, Y.; Xiao, B.; Wu, X.; Zhang, G. Magnetic yolk-shell structure of ZnFe<sub>2</sub>O<sub>4</sub> nanoparticles for enhanced visible light photo-Fenton degradation towards antibiotics and mechanism study. *Appl. Surf. Sci.* **2020**, *513*, 145820. [\[CrossRef\]](#)
- Dutta, J.; Mala, A.A. Removal of antibiotic from the water environment by the adsorption technologies: A review. *Water Sci. Technol.* **2020**, *82*, 401–426. [\[CrossRef\]](#) [\[PubMed\]](#)
- Priya, S.S.; Radha, K.V. A Review on the Adsorption Studies of Tetracycline onto Various Types of Adsorbents. *Chem. Eng. Commun.* **2017**, *204*, 821–839. [\[CrossRef\]](#)
- Krasucka, P.; Pan, B.; Ok, Y.S.; Mohan, D.; Sarkar, B.; Oleszczuk, P. Engineered biochar—A sustainable solution for the removal of antibiotics from water. *Chem. Eng. J.* **2021**, *405*, 126926. [\[CrossRef\]](#)
- Choi, K.-J.; Kim, S.-G.; Kim, S.-H. Removal of antibiotics by coagulation and granular activated carbon filtration. *J. Hazard. Mater.* **2008**, *151*, 38–43. [\[CrossRef\]](#)
- Saitoh, T.; Shibata, K.; Fujimori, K.; Ohtani, Y. Rapid removal of tetracycline antibiotics from water by coagulation-flotation of sodium dodecyl sulfate and poly(allylamine hydrochloride) in the presence of Al(III) ions. *Sep. Purif. Technol.* **2017**, *187*, 76–83. [\[CrossRef\]](#)
- Munoz, M.; de Pedro, Z.M.; Casas, J.A.; Rodriguez, J.J. Preparation of magnetite-based catalysts and their application in heterogeneous Fenton oxidation—A review. *Appl. Catal. B Environ.* **2015**, *176–177*, 249–265. [\[CrossRef\]](#)
- Wang, N.; Zheng, T.; Zhang, G.; Wang, P. A review on Fenton-like processes for organic wastewater treatment. *J. Environ. Chem. Eng.* **2016**, *4*, 762–787. [\[CrossRef\]](#)
- Ameta, R.; Chohadia, A.K.; Jain, A.; Punjabi, P.B. Fenton and Photo-Fenton Processes. In *Advanced Oxidation Processes for Waste Water Treatment*; Chapter 3; Ameta, S.C., Ameta, R., Eds.; Academic Press: Cambridge, MA, USA, 2018; pp. 49–87.
- Martínez, F.; Molina, R.; Rodríguez, I.; Pariente, M.I.; Segura, Y.; Melero, J.A. Techno-Economical assessment of coupling Fenton/biological processes for the treatment of a pharmaceutical wastewater. *J. Environ. Chem. Eng.* **2018**, *6*, 485–494. [\[CrossRef\]](#)
- Li, X.; Cui, K.; Guo, Z.; Yang, T.; Cao, Y.; Xiang, Y.; Chen, H.; Xi, M. Heterogeneous Fenton-like degradation of tetracyclines using porous magnetic chitosan microspheres as an efficient catalyst compared with two preparation methods. *Chem. Eng. J.* **2020**, *379*, 122324. [\[CrossRef\]](#)
- Lian, J.; Ouyang, Q.; Tsang, P.E.; Fang, Z. Fenton-like catalytic degradation of tetracycline by magnetic palygorskite nanoparticles prepared from steel pickling waste liquor. *Appl. Clay Sci.* **2019**, *182*, 105273. [\[CrossRef\]](#)
- Nie, M.; Li, Y.; He, J.; Xie, C.; Wu, Z.; Sun, B.; Zhang, K.; Kong, L.; Liu, J. Degradation of tetracycline in water using Fe<sub>3</sub>O<sub>4</sub> nanospheres as Fenton-like catalysts: Kinetics, mechanisms and pathways. *New J. Chem.* **2020**, *44*, 2847–2857. [\[CrossRef\]](#)

16. Du, D.; Shi, W.; Wang, L.; Zhang, J. Yolk-Shell structured  $\text{Fe}_3\text{O}_4@\text{void}@\text{TiO}_2$  as a photo-Fenton-like catalyst for the extremely efficient elimination of tetracycline. *Appl. Catal. B Environ.* **2017**, *200*, 484–492. [\[CrossRef\]](#)
17. Xu, J.; Liu, Z.; Zhao, D.; Gao, N.; Fu, X. Enhanced adsorption of perfluorooctanoic acid (PFOA) from water by granular activated carbon supported magnetite nanoparticles. *Sci. Total Environ.* **2020**, *723*, 137757. [\[CrossRef\]](#)
18. Du, C.; Song, Y.; Shi, S.; Jiang, B.; Yang, J.; Xiao, S. Preparation and characterization of a novel  $\text{Fe}_3\text{O}_4$ -graphene-biochar composite for crystal violet adsorption. *Sci. Total Environ.* **2020**, *711*, 134662. [\[CrossRef\]](#)
19. Li, Y.; Zimmerman, A.R.; He, F.; Chen, J.; Han, L.; Chen, H.; Hu, X.; Gao, B. Solvent-Free synthesis of magnetic biochar and activated carbon through ball-mill extrusion with  $\text{Fe}_3\text{O}_4$  nanoparticles for enhancing adsorption of methylene blue. *Sci. Total Environ.* **2020**, *722*, 137972. [\[CrossRef\]](#)
20. Qu, L.; Han, T.; Luo, Z.; Liu, C.; Mei, Y.; Zhu, T. One-Step fabricated  $\text{Fe}_3\text{O}_4@\text{C}$  core-shell composites for dye removal: Kinetics, equilibrium and thermodynamics. *J. Phys. Chem. Solids* **2015**, *78*, 20–27. [\[CrossRef\]](#)
21. Ai, L.; Zhang, C.; Liao, F.; Wang, Y.; Li, M.; Meng, L.; Jiang, J. Removal of methylene blue from aqueous solution with magnetite loaded multi-wall carbon nanotube: Kinetic, isotherm and mechanism analysis. *J. Hazard. Mater.* **2011**, *198*, 282–290. [\[CrossRef\]](#)
22. Dong, Y.; Cui, X.; Lu, X.; Jian, X.; Xu, Q.; Tan, C. Enhanced degradation of sulfadiazine by novel  $\beta$ -alaninediacetic acid-modified  $\text{Fe}_3\text{O}_4$  nanocomposite coupled with peroxymonosulfate. *Sci. Total Environ.* **2019**, *662*, 490–500. [\[CrossRef\]](#) [\[PubMed\]](#)
23. Ma, M.; Hou, P.; Zhang, P.; Cao, J.; Liu, H.; Yue, H.; Tian, G.; Feng, S. Magnetic  $\text{Fe}_3\text{O}_4$  nanoparticles as easily separable catalysts for efficient catalytic transfer hydrogenation of biomass-derived furfural to furfuryl alcohol. *Appl. Catal. A Gen.* **2020**, *602*, 117709. [\[CrossRef\]](#)
24. Ma, C.; Jia, S.; Yuan, P.; He, Z. Catalytic ozonation of 2,2'-methylenebis (4-methyl-6-tert-butylphenol) over nano- $\text{Fe}_3\text{O}_4@\text{cow dung ash}$  composites: Optimization, toxicity, and degradation mechanisms. *Environ. Pollut.* **2020**, *265*, 114597. [\[CrossRef\]](#) [\[PubMed\]](#)
25. Yu, X.; Lin, X.; Li, W.; Feng, W. Effective Removal of Tetracycline by Using Biochar Supported  $\text{Fe}_3\text{O}_4$  as a UV-Fenton Catalyst. *Chem. Res. Chin. Univ.* **2019**, *35*, 79–84. [\[CrossRef\]](#)
26. Plakas, K.V.; Mantza, A.; Sklari, S.D.; Zaspalis, V.T.; Karabelas, A.J. Heterogeneous Fenton-like oxidation of pharmaceutical diclofenac by a catalytic iron-oxide ceramic microfiltration membrane. *Chem. Eng. J.* **2019**, *373*, 700–708. [\[CrossRef\]](#)
27. Poza-Nogueiras, V.; Rosales, E.; Pazos, M.; Sanromán, M.Á. Current advances and trends in electro-Fenton process using heterogeneous catalysts—A review. *Chemosphere* **2018**, *201*, 399–416. [\[CrossRef\]](#)
28. Xu, L.; Wang, J. Magnetic Nanoscaled  $\text{Fe}_3\text{O}_4/\text{CeO}_2$  Composite as an Efficient Fenton-Like Heterogeneous Catalyst for Degradation of 4-Chlorophenol. *Environ. Sci. Technol.* **2012**, *46*, 10145–10153. [\[CrossRef\]](#)
29. Do, Q.C.; Kim, D.-G.; Ko, S.-O. Catalytic activity enhancement of a  $\text{Fe}_3\text{O}_4@\text{SiO}_2$  yolk-shell structure for oxidative degradation of acetaminophen by decoration with copper. *J. Clean. Prod.* **2018**, *172*, 1243–1253. [\[CrossRef\]](#)
30. Fatimah, I.; Amaliah, S.N.; Andrian, M.F.; Handayani, T.P.; Nurillahi, R.; Prakoso, N.I.; Wicaksono, W.P.; Chuenchom, L. Iron oxide nanoparticles supported on biogenic silica derived from bamboo leaf ash for rhodamine B photodegradation. *Sustain. Chem. Pharm.* **2019**, *13*, 100149. [\[CrossRef\]](#)
31. Chen, W.-H.; Huang, J.-R.; Lin, C.-H.; Huang, C.-P. Catalytic degradation of chlorpheniramine over  $\text{GO-Fe}_3\text{O}_4$  in the presence of  $\text{H}_2\text{O}_2$  in water: The synergistic effect of adsorption. *Sci. Total Environ.* **2020**, *736*, 139468. [\[CrossRef\]](#)
32. Hu, X.; Liu, B.; Deng, Y.; Chen, H.; Luo, S.; Sun, C.; Yang, P.; Yang, S. Adsorption and heterogeneous Fenton degradation of 17 $\alpha$ -methyltestosterone on nano  $\text{Fe}_3\text{O}_4$ /MWCNTs in aqueous solution. *Appl. Catal. B Environ.* **2011**, *107*, 274–283. [\[CrossRef\]](#)
33. Yoo, S.H.; Jang, D.; Joh, H.-I.; Lee, S. Iron oxide/porous carbon as a heterogeneous Fenton catalyst for fast decomposition of hydrogen peroxide and efficient removal of methylene blue. *J. Mater. Chem. A* **2017**, *5*, 748–755. [\[CrossRef\]](#)
34. Yang, Y.; Zhang, X.; Chen, Q.; Li, S.; Chai, H.; Huang, Y. Ultrasound-Assisted Removal of Tetracycline by a Fe/N-C Hybrids/ $\text{H}_2\text{O}_2$  Fenton-like System. *ACS Omega* **2018**, *3*, 15870–15878. [\[CrossRef\]](#) [\[PubMed\]](#)
35. Wang, X.; Xie, Y.; Ma, J.; Ning, P. Facile assembly of novel g-C $_3$ N $_4$ @expanded graphite and surface loading of nano zero-valent iron for enhanced synergistic degradation of tetracycline. *RSC Adv.* **2019**, *9*, 34658–34670. [\[CrossRef\]](#)
36. Wu, Q.; Yang, H.; Kang, L.; Gao, Z.; Ren, F. Fe-Based metal-organic frameworks as Fenton-like catalysts for highly efficient degradation of tetracycline hydrochloride over a wide pH range: Acceleration of Fe(II)/Fe(III) cycle under visible light irradiation. *Appl. Catal. B Environ.* **2020**, *263*, 118282. [\[CrossRef\]](#)
37. Ma, S.; Jing, J.; Liu, P.; Li, Z.; Jin, W.; Xie, B.; Zhao, Y. High selectivity and effectiveness for removal of tetracycline and its related drug resistance in food wastewater through schwertmannite/graphene oxide catalyzed photo-Fenton-like oxidation. *J. Hazard. Mater.* **2020**, *392*, 122437. [\[CrossRef\]](#)
38. Khodadadi, M.; Panahi, A.H.; Al-Musawi, T.J.; Ehrampoush, M.H.; Mahvi, A.H. The catalytic activity of  $\text{FeNi}_3@\text{SiO}_2$  magnetic nanoparticles for the degradation of tetracycline in the heterogeneous Fenton-like treatment method. *J. Water Process Eng.* **2019**, *32*, 100943. [\[CrossRef\]](#)
39. To, L.S.; Seebaluck, V.; Leach, M. Future energy transitions for bagasse cogeneration: Lessons from multi-level and policy innovations in Mauritius. *Energy Res. Soc. Sci.* **2018**, *35*, 68–77. [\[CrossRef\]](#)
40. Stanmore, B.R. Generation of Energy from Sugarcane Bagasse by Thermal Treatment. *Waste Biomass Valorization* **2010**, *1*, 77–89. [\[CrossRef\]](#)
41. Wakamura, Y. Utilization of Bagasse Energy in Thailand. *Mitig. Adapt. Strateg. Glob. Chang.* **2003**, *8*, 253–260. [\[CrossRef\]](#)
42. Tonnayopas, D. Green Building Bricks Made with Clays and Sugar Cane Bagasse Ash. In Proceedings of the 11th International Conference on Mining, Materials and Petroleum Engineering, Sinaia, Romania, 17–19 January 2013.



43. Rattanachueskul, N.; Saring, A.; Kaowphong, S.; Chumha, N.; Chuenchom, L. Magnetic carbon composites with a hierarchical structure for adsorption of tetracycline, prepared from sugarcane bagasse via hydrothermal carbonization coupled with simple heat treatment process. *Bioresour. Technol.* **2017**, *226*, 164–172. [[CrossRef](#)] [[PubMed](#)]
44. Novais, R.M.; Ascensão, G.; Tobaldi, D.M.; Seabra, M.P.; Labrincha, J.A. Biomass fly ash geopolymer monoliths for effective methylene blue removal from wastewaters. *J. Clean. Prod.* **2018**, *171*, 783–794. [[CrossRef](#)]
45. Le Blond, J.S.; Woskie, S.; Horwell, C.J.; Williamson, B.J. Particulate matter produced during commercial sugarcane harvesting and processing: A respiratory health hazard? *Atmos. Environ.* **2017**, *149*, 34–46. [[CrossRef](#)]
46. Rodríguez-Díaz, J.; García, J.; Sánchez, L.; Silva, M.; Silva, V.; Arteaga-Pérez, L. Comprehensive Characterization of Sugarcane Bagasse Ash for Its Use as an Adsorbent. *Bioenergy Res.* **2015**, *8*, 1885–1895. [[CrossRef](#)]
47. Madurwar, M.; Mandavgane, S.; Ralegaonkar, R. Use of sugarcane bagasse ash as brick material. *Curr. Sci.* **2014**, *117*, 1044–1051.
48. Xu, Q.; Ji, T.; Gao, S.-J.; Yang, Z.; Wu, N. Characteristics and Applications of Sugar Cane Bagasse Ash Waste in Cementitious Materials. *Materials* **2018**, *12*, 39. [[CrossRef](#)]
49. Sales, A.; Lima, S.A. Use of Brazilian sugarcane bagasse ash in concrete as sand replacement. *Waste Manag.* **2010**, *30*, 1114–1122. [[CrossRef](#)]
50. Webber, C.P., Jr.; Spaunhorst, D.; Petrie, E. Impact of Sugarcane Bagasse Ash as an Amendment on the Physical Properties, Nutrient Content and Seedling Growth of a Certified Organic Greenhouse Growing Media. *J. Agric. Sci.* **2017**, *9*, 1. [[CrossRef](#)]
51. Purnomo, C.W.; Respito, A.; Sitanggang, E.P.; Mulyono, P. Slow release fertilizer preparation from sugar cane industrial waste. *Environ. Technol. Innov.* **2018**, *10*, 275–280. [[CrossRef](#)]
52. Mane, V.S.; Mall, I.D.; Srivastava, V.C. Use of bagasse fly ash as an adsorbent for the removal of brilliant green dye from aqueous solution. *Dyes Pigment.* **2007**, *73*, 269–278. [[CrossRef](#)]
53. Gaikwad, D.R. Low cost Sugarcane Bagasse Ash as an Adsorbent for Dye Removal from Dye Effluent. *Int. J. Chem. Eng. Appl.* **2010**, *1*, 309–318.
54. Mor, S.; Negi, P.; Ravindra, K. Potential of agro-waste sugarcane bagasse ash for the removal of ammoniacal nitrogen from landfill leachate. *Environ. Sci. Pollut. Res.* **2019**, *26*, 24516–24531. [[CrossRef](#)] [[PubMed](#)]
55. Abdul Mutalib, A.A.; Ibrahim, M.L.; Matmin, J.; Kassim, M.F.; Mastuli, M.S.; Taufiq-Yap, Y.H.; Shohaimi, N.A.M.; Islam, A.; Tan, Y.H.; Kaus, N.H.M. SiO<sub>2</sub>-Rich Sugar Cane Bagasse Ash Catalyst for Transesterification of Palm Oil. *Bioenergy Res.* **2020**, *13*, 986–997. [[CrossRef](#)]
56. Meng, Q.; Xiang, S.; Zhang, K.; Wang, M.; Bu, X.; Xue, P.; Liu, L.; Sun, H.; Yang, B. A facile two-step etching method to fabricate porous hollow silica particles. *J. Colloid Interface Sci.* **2012**, *384*, 22–28. [[CrossRef](#)]
57. Park, J.; Han, Y.; Kim, H. Formation of Mesoporous Materials from Silica Dissolved in Various NaOH Concentrations: Effect of pH and Ionic Strength. *J. Nanomater.* **2012**, *2012*, 528174. [[CrossRef](#)]
58. Clark, M.W.; Despland, L.M.; Lake, N.J.; Yee, L.H.; Anstoetz, M.; Arif, E.; Parr, J.F.; Doumit, P. High-efficiency cogeneration boiler bagasse-ash geochemistry and mineralogical change effects on the potential reuse in synthetic zeolites, geopolymers, cements, mortars, and concretes. *Heliyon* **2017**, *3*, e00294. [[CrossRef](#)]
59. Subramanian, V.; Ordonsky, V.V.; Legras, B.; Cheng, K.; Cordier, C.; Chernavskii, P.A.; Khodakov, A.Y. Design of iron catalysts supported on carbon–silica composites with enhanced catalytic performance in high-temperature Fischer–Tropsch synthesis. *Catal. Sci. Technol.* **2016**, *6*, 4953–4961. [[CrossRef](#)]
60. Ma, S.; Gu, J.; Han, Y.; Gao, Y.; Zong, Y.; Ye, Z.; Xue, J. Facile Fabrication of C–TiO<sub>2</sub> Nanocomposites with Enhanced Photocatalytic Activity for Degradation of Tetracycline. *ACS Omega* **2019**, *4*, 21063–21071. [[CrossRef](#)]
61. Zhu, X.; Qian, F.; Liu, Y.; Matera, D.; Wu, G.; Zhang, S.; Chen, J. Controllable synthesis of magnetic carbon composites with high porosity and strong acid resistance from hydrochar for efficient removal of organic pollutants: An overlooked influence. *Carbon* **2016**, *99*, 338–347. [[CrossRef](#)]
62. Mohan, D.; Sarswat, A.; Singh, V.K.; Alexandre-Franco, M.; Pittman, C.U. Development of magnetic activated carbon from almond shells for trinitrophenol removal from water. *Chem. Eng. J.* **2011**, *172*, 1111–1125. [[CrossRef](#)]
63. Pompe, C.E.; Slagter, M.; de Jongh, P.E.; de Jong, K.P. Impact of heterogeneities in silica-supported copper catalysts on their stability for methanol synthesis. *J. Catal.* **2018**, *365*, 1–9. [[CrossRef](#)]
64. Lai, C.; Huang, F.; Zeng, G.; Huang, D.; Qin, L.; Cheng, M.; Zhang, C.; Li, B.; Yi, H.; Liu, S.; et al. Fabrication of novel magnetic MnFe<sub>2</sub>O<sub>4</sub>/bio-char composite and heterogeneous photo-Fenton degradation of tetracycline in near neutral pH. *Chemosphere* **2019**, *224*, 910–921. [[CrossRef](#)] [[PubMed](#)]
65. Ma, X.; Cheng, Y.; Ge, Y.; Wu, H.; Li, Q.; Gao, N.; Deng, J. Ultrasound-enhanced nanosized zero-valent copper activation of hydrogen peroxide for the degradation of norfloxacin. *Ultrason. Sonochem.* **2018**, *40*, 763–772. [[CrossRef](#)] [[PubMed](#)]
66. Hou, L.; Wang, L.; Royer, S.; Zhang, H. Ultrasound-assisted heterogeneous Fenton-like degradation of tetracycline over a magnetite catalyst. *J. Hazard. Mater.* **2016**, *302*, 458–467. [[CrossRef](#)]
67. Gan, Q.; Hou, H.; Liang, S.; Qiu, J.; Tao, S.; Yang, L.; Yu, W.; Xiao, K.; Liu, B.; Hu, J.; et al. Sludge-Derived biochar with multivalent iron as an efficient Fenton catalyst for degradation of 4-Chlorophenol. *Sci. Total Environ.* **2020**, *725*, 138299. [[CrossRef](#)]
68. Tang, J.; Wang, J. Fenton-like degradation of sulfamethoxazole using Fe-based magnetic nanoparticles embedded into mesoporous carbon hybrid as an efficient catalyst. *Chem. Eng. J.* **2018**, *351*, 1085–1094. [[CrossRef](#)]

69. Nitoi, I.; Oancea, P.; Constantin, L.A.; Raileanu, M.; Crisan, M.; Cristea, I.; Cosma, C. Relationship between structure of some nitroaromatic pollutants and their degradation kinetic parameters in UV-VIS./TiO<sub>2</sub> system. *J. Environ. Prot. Ecol.* **2016**, *17*, 315–322.
70. Wang, X.; Zhuang, Y.; Zhang, J.; Song, L.; Shi, B. Pollutant degradation behaviors in a heterogeneous Fenton system through Fe/S-doped aerogel. *Sci. Total Environ.* **2020**, *714*, 136436. [[CrossRef](#)]
71. Qiu, Y.; Xu, X.; Xu, Z.; Liang, J.; Yu, Y.; Cao, X. Contribution of different iron species in the iron-biochar composites to sorption and degradation of two dyes with varying properties. *Chem. Eng. J.* **2020**, *389*, 124471. [[CrossRef](#)]
72. Javid, A.; Mesdaghinia, A.; Nasser, S.; Mahvi, A.H.; Alimohammadi, M.; Gharibi, H. Assessment of tetracycline contamination in surface and groundwater resources proximal to animal farming houses in Tehran, Iran. *J. Environ. Health Sci. Eng.* **2016**, *14*, 4. [[CrossRef](#)]
73. Saygılı, H.; Güzel, F. Effective removal of tetracycline from aqueous solution using activated carbon prepared from tomato (*Lycopersicon esculentum* Mill.) industrial processing waste. *Ecotoxicol. Environ. Saf.* **2016**, *131*, 22–29. [[CrossRef](#)] [[PubMed](#)]
74. Chen, Z.; Mu, D.; Chen, F.; Tan, N. NiFe<sub>2</sub>O<sub>4</sub>@ nitrogen-doped carbon hollow spheres with highly efficient and recyclable adsorption of tetracycline. *RSC Adv.* **2019**, *9*, 10445–10453. [[CrossRef](#)]
75. Chang, P.H.; Li, Z.; Jean, J.S.; Jiang, W.T.; Wu, Q.; Kuo, C.Y.; Kraus, J. Desorption of tetracycline from montmorillonite by aluminum, calcium, and sodium: An indication of intercalation stability. *Int. J. Environ. Sci. Technol.* **2014**, *11*, 633–644. [[CrossRef](#)]